### Macroscopically Degenerate Exactly Solvable Point in the Spin-1/2 Kagome Quantum Antiferromagnet

Hitesh J. Changlani, <sup>1,2,3</sup> Dmitrii Kochkov, <sup>3</sup> Krishna Kumar, <sup>3</sup> Bryan K. Clark, <sup>3</sup> and Eduardo Fradkin <sup>3</sup> Department of Physics and Astronomy, Johns Hopkins University, Baltimore, Maryland 21218, USA <sup>2</sup> Institute for Quantum Matter, Johns Hopkins University, Baltimore, Maryland 21218, USA <sup>3</sup> Department of Physics and Institute for Condensed Matter Theory, University of Illinois at Urbana-Champaign, 1110 West Green Street, Urbana Illinois 61801, USA

(Received 10 December 2017; published 13 March 2018)

Frustrated quantum magnets are a central theme in condensed matter physics due to the richness of their phase diagrams. They support a panoply of phases including various ordered states and topological phases. Yet, this problem has defied a solution for a long time due to the lack of controlled approximations which make it difficult to distinguish between competing phases. Here we report the discovery of a special quantum macroscopically degenerate point in the XXZ model on the spin-1/2 kagome quantum antiferromagnet for the ratio of Ising to antiferromagnetic transverse coupling  $J_z/J = -1/2$ . This point is proximate to many competing phases explaining the source of the complexity of the phase diagram. We identify five phases near this point including both spin-liquid and broken-symmetry phases and give evidence that the kagome Heisenberg antiferromagnet is close to a transition between two phases.

DOI: 10.1103/PhysRevLett.120.117202

The history of quantum frustrated magnetism began in 1973 with Anderson's suggestion that the ground state of the nearest-neighbor (NN) Heisenberg model on the triangular lattice was a quantum spin liquid [1]. While we now know that this particular model does not support a spin liquid, both experimental and theoretical evidence has been building for quantum spin liquids in various lattices built of triangular motifs. Materials such as herbertsmithite (a kagome lattice of Cu<sup>2+</sup> ions) [2] and Na<sub>4</sub>Ir<sub>3</sub>O<sub>8</sub> (a hyperkagome lattice of Ir<sup>4+</sup> ions) [3] fail to order down to low temperatures suggesting a possible spin-liquid ground state. This is supported by theoretical calculations which show that a panoply of spin liquids (or exotic ordered phases) occur in a variety of Hamiltonians [4–17]. This Letter presents an explanation of multiple energetically competitive phases in these models.

We first report the existence of a new macroscopic *quantum* degenerate point on kagome and hyperkagome lattices in the spin-1/2 XXZ Hamiltonian [18–23],

$$H_{XXZ}[J_z] = \sum_{\langle i,j \rangle} S_i^x S_j^x + S_i^y S_j^y + J_z \sum_{\langle i,j \rangle} S_i^z S_j^z \qquad (1)$$

at  $H_{XXZ}[-1/2]$  (notated as  $H_{XXZ0}$  [24]).  $S_i$  are spin-1/2 operators on site i,  $\langle i, j \rangle$  refer to nearest-neighbor pairs, and  $J_z$  is the Ising coupling. The degeneracy exists in all  $S_z$  sectors and all finite system sizes. For the kagome, we explicitly demonstrate this in Fig. 1 where we perform an exact diagonalization (ED) on the N=30 site kagome cluster in different  $S_z$  sectors. As we approach  $J_z=-1/2$ , many eigenstates collapse to the same ground state eigenvalue.

We solve analytically for much of the exponential manifold, and our solutions apply to any lattice of triangular motifs with the Hamiltonian of the form

$$H = \sum_{\Lambda} H_{XXZ0}(\Delta), \tag{2}$$

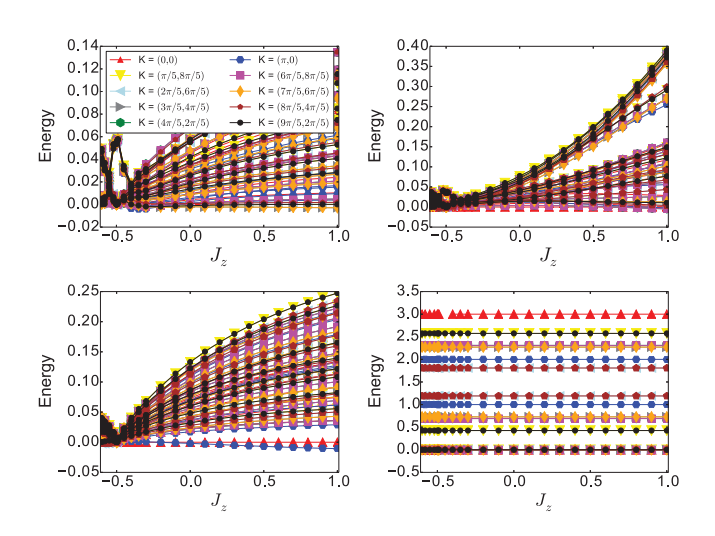


FIG. 1. Energy spectra [showing the eight lowest energies in every momentum sector with respect to the lowest energy state in K=(0,0)] versus  $J_z$  for a 30-site kagome cluster with periodic boundary conditions. The panels correspond to various  $S_z$  sectors, (top left)  $S_z=0$ , (top right)  $S_z=5$ , (bottom left)  $S_z=10$ , (bottom right)  $S_z=14$ . A quantum degeneracy is seen at  $J_z=-1/2$ . The case of  $S_z=14$  corresponds to one spin-down in a sea of up spins and maps to the noninteracting solution; hence, the spectrum does not change with  $J_z$ .

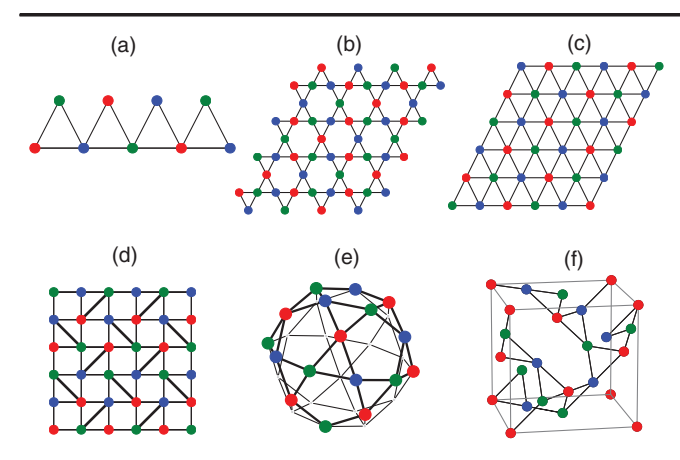


FIG. 2. Representative three-coloring solutions on various lattices with triangular motifs: (a) sawtooth, (b) kagome, (c) triangular, (d) Shastry-Sutherland [27] (with  $J_2 = 2J_1$ ; note, the bold diagonal lines are associated with two triangles, whereas other edges are part of only one triangle), (e) icosidodecahedron, (f) hyperkagome lattice.

where  $H_{XXZ0}(\Delta)$  is the XXZ0 Hamiltonian on a triangle  $\Delta$ , as long as its vertices can be colored by three colors with no two connected vertices being assigned the same color. Some three-colorable lattices with representative three colorings are shown in Fig. 2. Our general result overlaps the XXZ0 point on the triangular lattice of Ref. [25] and a different analytically solvable Hamiltonian on the zigzag ladder of Ref. [26].

Finally, we show how the *XXZ*0 point on the kagome lattice is embedded in the wider phase diagram demonstrating its relation to the previously discovered spin liquid at the Heisenberg point [7,8,10] as well as nearby magnetically ordered phases; our results suggest an additional intermediate phase transition in the middle of the spin-liquid region.

Exact ground states at  $J_z = -1/2$ .—Any Hamiltonian of the form of Eq. (2) has ground states of the form

$$|C\rangle \equiv P_{S_z} \left( \prod_{\text{valid}} \otimes |\gamma_s\rangle \right),$$
 (3)

where  $\{|\gamma_s\rangle=|a\rangle,|b\rangle$  or  $|c\rangle\}$  denoted as "colors" on site s are defined as  $|a\rangle\equiv(1/\sqrt{2})(|\uparrow\rangle+|\downarrow\rangle), |b\rangle\equiv(1/\sqrt{2})(|\uparrow\rangle+\omega|\downarrow\rangle), |c\rangle\equiv(1/\sqrt{2})(|\uparrow\rangle+\omega^2|\downarrow\rangle)$ , where  $\omega=e^{i2\pi/3}$ . Taking the quantization axis to be the z axis, the colors correspond to spin directions in the XY plane that are at 120° relative to one another. Valid colorings satisfy the three-coloring condition.  $P_{S_z}$  projects into a particular total  $S_z$  sector.

For  $J_z = -1/2$  and a single triangle, six states—the fully polarized state  $|\uparrow\uparrow\uparrow\rangle$  and the chiral states  $|\uparrow\downarrow\downarrow\rangle + \omega|\downarrow\uparrow$   $\downarrow\rangle + \omega^2|\downarrow\downarrow\uparrow\rangle$  and  $|\uparrow\downarrow\downarrow\rangle + \omega^2|\downarrow\uparrow\downarrow\uparrow\rangle$  and all their Kramers pairs—are exactly degenerate. Thus, Eq. (2) is recast as

$$H = \sum_{\Delta} H_{\Delta} = \frac{3}{2} \sum_{\Delta} P_{\Delta} - \frac{3}{8} N_{\Delta},\tag{4}$$

where  $N_{\Delta}$  is the number of triangles, and  $P_{\Delta}$  is a projector on the triangle  $P_{\Delta} \equiv |+\rangle\langle+|+|-\rangle\langle-|$ , and  $|+\rangle$  and  $|-\rangle$  are Kramers pairs of nonchiral one-magnon states on the triangle  $|+\rangle \equiv (1/\sqrt{3})(|\uparrow\uparrow\downarrow\rangle+|\uparrow\downarrow\rangle+|\downarrow\uparrow\uparrow\rangle)$  and  $|-\rangle \equiv (1/\sqrt{3})(|\downarrow\downarrow\uparrow\rangle+|\downarrow\uparrow\downarrow\rangle+|\uparrow\downarrow\downarrow\rangle)$ . This rewriting can be carried out on any lattice of triangles; if a bond is used by multiple triangles, this constrains the coupling constant between these bonds.

The *XXZ*0 Hamiltonian is, thus, a sum of positive semidefinite noncommuting projectors. Any wave function that simultaneously zeroes out each projector consistently is guaranteed to be a ground state. Such "frustration-free" Hamiltonians include Majumdar-Ghosh [28] (generalized by Klein [29]) and Affleck-Kennedy-Lieb-Tasaki [30–33] Hamiltonians. Zeroing out a projector requires that only components exactly orthogonal to states  $|+\rangle$  and  $|-\rangle$  enter the full many-body wave function; this is indeed achieved by the product state  $|\psi\rangle \equiv \prod_{\text{valid}} \otimes |\gamma_s\rangle$ . We also note that such "three-coloring states" have a long history and have been explored in several contexts [24,34–40].

The product state  $|\psi\rangle$  does not conserve total  $S_z$  but the XXZ Hamiltonian does conserve it. Therefore, projecting each three-coloring solution to each  $S_z$  sector is also a ground state leading to Eq. (3). Note that three colorings which differ simply by relabeling colors are identical up to a global phase (see the Supplemental Material [41]).

Macroscopic degeneracy and additional ground states.—While there are only two ways of three coloring the triangular lattice, there are an exponential number of ways of doing so on the kagome (scaling as  $1.208^N$  [42]) and hyperkagome lattices. The precise number of ground states varies from sector to sector because of the loss of linear independence of the unprojected solutions under projection. For typical  $S_z$  of interest, particularly  $S_z = 0$ , there are still an exponential number of linearly independent solutions. This counting is made precise by forming the overlap matrix  $S_{C,C'} \equiv \langle C|C'\rangle$  and evaluating its rank  $\equiv R(S)$  numerically; our results have been shown in Table I and the Supplemental Material [41]. The case of one down spin in a sea of up spins, which maps to the noninteracting problem with a flatband with a quadratic band touching [43], is also correctly captured.

On several representative clusters with open boundary conditions (but always with completed triangles), we never find solutions outside the coloring manifold, which suggests (but does not prove) the possibility that coloring solutions describe all degeneracies on open lattices. However, for the kagome on tori we find, for low fillings, degenerate solutions not spanned by colorings.

Connection to the wider kagome phase diagram.—We now show how the XXZ0 point is embedded in the larger kagome phase diagram. We focus on  $S_z = 0$  and the fully

TABLE I. Number of ground states in different  $S_z$  sectors (mapped to hard-core boson number  $n_b$ ) on several lattices (of size N) with triangular motifs at  $J_z = -1/2$ ,  $J_2 = 0$ . R(S) is the rank of the overlap matrix indicating the number of linearly independent three-coloring modes, and ED refers to the exact number of ground states. The kagome cluster with open boundary conditions (OBC) has completed triangles resembling the periodic counterpart (PBC) in appearance.

Lattice	Method	$n_b = 1$	$n_b = 2$	$n_b = 3$	$n_b = 4$	$n_b = 5$	$n_b = 6$	$n_b = \lfloor N/2 \rfloor$	Number of three colorings
Sawtooth OBC Five triangles	ED $R(S)$	6 6	16 16	26 26	31 31	32 32	32 32	32 32	32
3 × 3 kagome OBC (33 sites)	ED $R(S)$	15 15	102 102	414 414	1117 1117	2136	3078	3808	3808
3 × 3 kagome PBC	ED $R(S)$	10 10	38 34	60 40	41 40	40 40	40 40	40 40	40
4 × 3 kagome PBC	ED $R(S)$	13 13	68 68	169 134	172 136	137 136	136 136	136	136

symmetric sector of the K = (0,0) sector (see the Supplemental Material [41]) and study an extended Hamiltonian involving NN and next-nearest-neighbor (NNN) terms,

$$H[J_z, J_2] = H_{XXZ}^{NN}[J_z] + J_2 H_{XXZ}^{NNN}[J_z],$$
 (5)

where  $H_{XXZ}^{\rm NNN}[J_z] = (\sum_{\langle\langle i,j\rangle\rangle} S_i^x S_j^x + S_i^y S_j^y + J_z S_i^z S_j^z)$  with  $\langle\langle i,j\rangle\rangle$  referring to NNN pairs. We use a combination of analytical arguments and ED on the 36d cluster [44,45] on a grid of points in the  $(J_z,J_2)$  space. As Fig. 3 shows, we find five phases near XXZ0: a ferromagnetic phase, a q=0 phase, a  $\sqrt{3}\times\sqrt{3}$  phase, and (potentially) two spin liquids. We give numerical evidence that all these phases, other than the ferromagnet, connect from near (or touching) XXZ0 to the Heisenberg point.

At  $J_z=-1/2$  and  $J_2>0$  (notated as the AF line) all triangles in the Hamiltonian are of the *XXZ*0 form and remain consistently three colorable. Three coloring both NN and NNN triangles constrains the allowed colorings, leaving only two colorings in the well-known q=0 pattern. This phase survives for  $J_z>-1/2$  at small  $J_2$  and is primarily identified by peaks at the *M* point (see Fig. S2 of the Supplemental Material [41]) in the spin-structure factor  $S(\vec{q}) \equiv (1/N) \sum_{i,j} \langle S_i \cdot S_j \rangle e^{i\vec{q} \cdot (\vec{r}_i - \vec{r}_j)}$ , where  $\vec{r}_i$  refers to the real space coordinates of the *i*th lattice site, *N* is the total number of sites, and  $\langle S_i \cdot S_j \rangle$  is the spin-spin correlation function. On the other hand, it can be rigorously shown the minimum energy state upon perturbing the AF line to  $J_z < -1/2$  is the fully polarized ferromagnetic state.

At  $J_z = -1/2$  and  $J_2 < 0$ , we find evidence for the  $\sqrt{3} \times \sqrt{3}$  phase. While we cannot solve for the exact ground state, the state which colors NNN triangles with the same color (i.e., the  $\sqrt{3} \times \sqrt{3}$  phase) minimizes the NNN energy within the three-coloring manifold. We numerically verify this phase by looking at S(K), finding it survives for  $J_z$  near and on both sides of -1/2.

By tracing paths through parameter space with large values of  $S(\vec{q})$  at the K and M points, we find that both the q=0 phase and  $\sqrt{3} \times \sqrt{3}$  phases near the XXZO point extend to the Heisenberg point at nonzero  $J_2$ . To locate the boundaries of these phases, we perform sweeps through  $J_2$ 

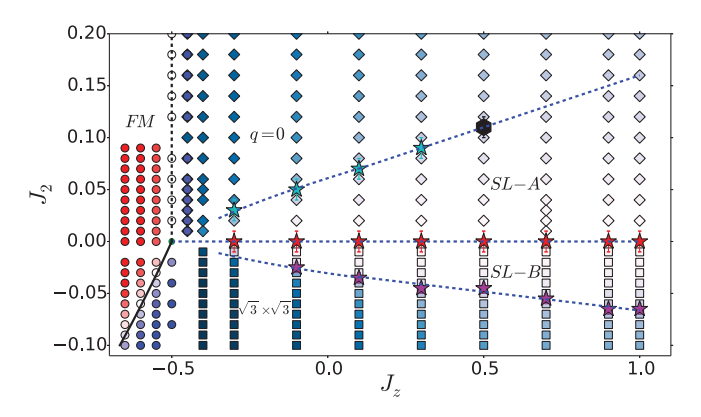


FIG. 3. The phase diagram in the  $J_z - J_2$  plane on the 36d lattice showing five phases: the ferromagnet (FM), the magnetically ordered phases  $(q = 0 \text{ and } \sqrt{3} \times \sqrt{3})$ , and the spin liquids (SL-A and SL-B). Circles correspond to the energy difference  $E(S_z = 0)_{N=36} - E_{TDL}(S_z = N/2)$  between the  $S_z = 0$  sector and fully polarized state ranging from deep blue (negative) to deep red (positive). The diamonds are colored based on the structure factor at the M point [S(M)] and squares are colored based on the structure factor at the K point [S(K)]. The darkest color corresponds to the largest structure factor on the graph. Star symbols correspond to the location of fidelity dips, and the error bars indicate the uncertainty in the location of the phase boundaries (when scanned in the  $J_2$  direction) and correspond to the grid spacing used for the computation of the fidelity. The black hexagon (at  $J_z \approx 0.5$ ,  $J_2 \approx 0.10$ ) is a kink in the second derivative of the fidelity; beyond the corresponding  $J_z$ , the fidelity dip is not noticeable, and the phase boundary is just an extrapolation. Phase boundaries are marked with dotted lines, which are guides to the eye. The solid line is where the semiclassical energy difference between the FM and the unprojected  $\sqrt{3} \times \sqrt{3}$  state goes to zero.

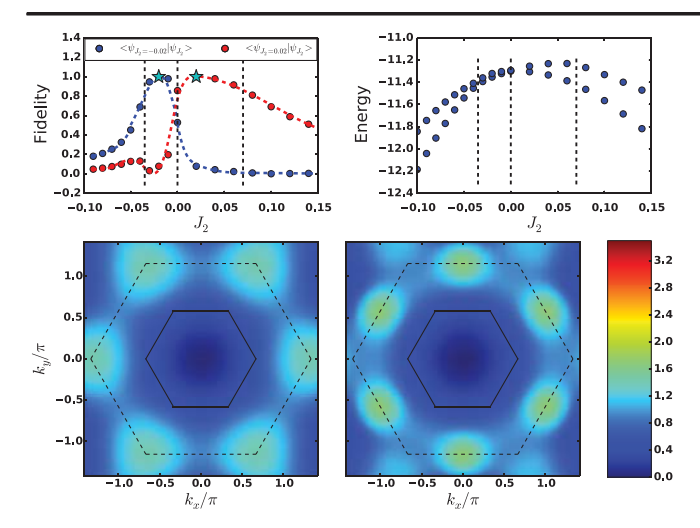


FIG. 4. All data are at  $J_z=0.1$  for the 36d lattice. Top left: Overlap of the ground state at  $J_2$  with respect to reference ground state wave functions at  $J_2=-0.02$  (blue) and  $J_2=0.02$  (red). Dashed lines represent transitions as measured by fidelity. Top right: Energy of the two lowest states in the symmetric representation of the K=(0,0) sector. There are additional state(s) between these two states in other quantum-number sectors. Bottom: The static spin-structure factor  $S(\vec{q})$  of the ground state for  $J_2=-0.02$  (left) and  $J_2=0.02$  (right). The solid and the dotted lines show the first and the extended Brillouin zones, respectively. The high symmetry points of the latter correspond to K (corners of the hexagon) and M (midpoints of edges) points. On going from  $J_2<0$  to  $J_2>0$ , the intensity is transferred from K to M points.

at fixed  $J_z$  and identify dips in the wave function fidelity defined to be

$$f(J_z, J_2) \equiv |\langle \psi(J_z, J_2 - \Delta J_2/2)|\psi(J_z, J_2 + \Delta J_2/2)\rangle|,$$
 (6)

where  $\psi(J_z,J_2)$  is the ground state wave function, and  $\Delta J_2$  is the step size in the  $J_2$  direction. For both magnetically ordered phases, the location of these dips form lines emanating from (or close to) the XXZ0 point that extrapolate to the Heisenberg point ( $J_z=1$ ) to values  $J_2\approx 0.16$  for q=0 and  $J_2\approx -0.06$  for  $\sqrt{3}\times\sqrt{3}$ . These values are within the bounds previously found by a density matrix renormalization group study [46] but disagree with a variational study by Ref. [47], which finds instead a valence bond crystal. In the intermediate phase(s), we see a decrease in the magnitude of the structure factor peaks consistent with a change in phase to a spin liquid.

Near XXZ0, we do not detect fidelity dips and see larger structure factors that extend much closer to the line  $J_2 = 0$ . This leaves two plausible scenarios: (1) the spin liquid(s) terminate at  $J_z > -1/2$  for all  $J_2$ , or (2) the phase boundaries extend to XXZ0 but finite size effects near it become large making it difficult to resolve the transition.

We find an additional fidelity dip at  $J_2 \approx 0$  and  $J_z > -1/2$  in the region where other studies [46] identify

a single spin-liquid phase. This interesting finding indicates the existence of an additional transition in this region. Our analysis in this work is largely ambivalent about the nature of these two phases, but earlier evidence for a spin-liquid phase at  $J_z=1$  and both  $J_2>0$ ,  $J_2<0$  [14,46] suggests a possible transition between two spin liquids. Interestingly, a recent IPEPS study [48] found nearly degenerate variational degenerate energies for the  $Q_1=Q_2$  and  $Q_1=-Q_2$  [38]  $Z_2$ -spin liquids which they interpret as evidence for a parent U(1) Dirac spin liquid; given our results, another reasonable interpretation is that there is a transition between these two states.

To further understand the nature of the fidelity dips, we consider the ground state and excited state in the same quantum-number sector as a function of  $J_2$  at  $J_z = 0.1$  (Fig. 4, top right); the true first excited state is in another sector. We see a (formally avoided) "level crossing" indicated by a shrinking gap between these states around  $J_2 \approx 0$ . This crossing causes the fidelity dip and leads to the overlap of the wave function on both sides of  $J_2 \approx 0$  being small with respect to a reference point on the other side (see Fig. 4, top left). In addition, the structure factors of the two ground states at positive and negative  $J_2$ , despite not having large peaks, are qualitatively distinct (see Fig. 4, bottom).

Conclusion.—In summary, we have shown that (1)  $H_{XXZ0}$  is macroscopically quantum degenerate on the kagome and hyperkagome lattices, (2) all projected threecoloring states are exact ground states of  $H_{XXZ0}$  on any three-colorable lattice of triangular motifs explaining this macroscopic degeneracy, (3) multiple phases in the  $J_2 - J_z$ phase diagram, including spin liquid(s) in the Heisenberg regime, are proximate to the XXZ0 point, and (4) we have given evidence for a transition between two phases at  $J_2 =$ 0 for  $-0.5 < J_z < 1$ . Our findings suggest that the XXZ0 point controls the physics of the Heisenberg and XY points [15,49] on the kagome, and the existence of a transition near the Heisenberg point might help resolve conflicting numerical evidence for gapless and gapped states, respectively. While our focus here has been on the uniform kagome lattice, the exponential degeneracy also applies in the case where the coupling constant in each triangle is disordered (or staggered) as well as to finite clusters of triangles such as the icosidodecahedron; in fact, the latter explains the nearly degenerate manifold on this cluster in the XY regime [50].

The central coloring ideas extend to other frustrated lattices with four (or higher) site motifs [51–53]. For example, define a Hamiltonian which annihilates four-coloring states made of one  $a \equiv |\uparrow\rangle + |\downarrow\rangle$ ,  $b \equiv |\uparrow\rangle + i|\downarrow\rangle$ ,  $c \equiv |\uparrow\rangle - |\downarrow\rangle$ , and  $d \equiv |\uparrow\rangle - i|\downarrow\rangle$  on each square of a square lattice or tetrahedron of the pyrochlore lattice. Up to a constant, this is  $H = 2H_{XXZ}[-1/4] + \sum_{i < j,k < l,\text{diff}} S_i^+ S_j^+ S_k^- S_l^- - 2S_1^z S_2^z S_3^z S_4^z$  where "diff" indicates i,j,k,l are distinct (see the Supplemental Material for the derivation that used the DiracQ package [54]). Notice that

on the square, this forces the NNN  $J_2$  coupling to be half the NN  $J_1$  coupling; interestingly,  $J_2/J_1 = 1/2$  has been proposed to be a SL state on the square for Heisenberg and XY models [55]. We believe that the macroscopic degeneracy of this Hamiltonian on the square and pyrochlore lattices will be a source of multiple phases on these lattices [56,57].

Finally, we note that three-coloring states can be used to construct accurate many-body wave functions [12,58–60]. Typically, Jastrow factors have been introduced only on top of a single coloring; our present investigation suggests that a linear combination of colorings may provide accurate results in the vicinity of the *XXZ*0 point.

We thank V. Elser, S. Shastry, O. Tchernyshyov, V. Chua, L. D.C Jaubert, S. Sachdev, R. Flint, P. Nikolic, Y. Wan, and O. Benton for discussions and H. Wang for collaboration on related work. We also thank T. Momoi for bringing to our attention Ref. [25] after this work was posted. H. J. C., D. K., and B. K. C. were supported by SciDAC Grant No. DE-FG02-12ER46875 and K. K. and E. F. by NSF Grants No. DMR 1408713 and No. 1725401. H. J. C. also acknowledges funding from the U.S. Department of Energy, Office of Basic Energy Sciences, Division of Materials Sciences and Engineering under Award No. DE-FG02-08ER46544 for his work at the Institute for Quantum Matter. This research is part of the Blue Waters sustained petascale computing project, which is supported by the National Science Foundation (Grants No. OCI-0725070 and No. ACI-1238993) and the State of Illinois.

- [1] P. Anderson, Mater. Res. Bull. 8, 153 (1973).
- [2] J. S. Helton, K. Matan, M. P. Shores, E. A. Nytko, B. M. Bartlett, Y. Yoshida, Y. Takano, A. Suslov, Y. Qiu, J.-H. Chung, D. G. Nocera, and Y. S. Lee, Phys. Rev. Lett. 98, 107204 (2007).
- [3] Y. Okamoto, M. Nohara, H. Aruga-Katori, and H. Takagi, Phys. Rev. Lett. 99, 137207 (2007).
- [4] C. Zeng and V. Elser, Phys. Rev. B 42, 8436 (1990).
- [5] R. R. P. Singh and D. A. Huse, Phys. Rev. B 76, 180407 (2007).
- [6] Y. Ran, M. Hermele, P. A. Lee, and X.-G. Wen, Phys. Rev. Lett. 98, 117205 (2007).
- [7] S. Yan, D. A. Huse, and S. R. White, Science 332, 1173 (2011).
- [8] S. Depenbrock, I. P. McCulloch, and U. Schollwöck, Phys. Rev. Lett. 109, 067201 (2012).
- [9] Y. Iqbal, F. Becca, S. Sorella, and D. Poilblanc, Phys. Rev. B 87, 060405 (2013).
- [10] H.-C. Jiang, Z. Wang, and L. Balents, Nat. Phys. 8, 902 (2012).
- [11] B. K. Clark, J. M. Kinder, E. Neuscamman, Garnet Kin-Lic Chan, and M. J. Lawler, Phys. Rev. Lett. 111, 187205 (2013).
- [12] T. Tay and O. I. Motrunich, Phys. Rev. B **84**, 020404 (2011).

- [13] Y.-C. He, M. P. Zaletel, M. Oshikawa, and F. Pollmann, Phys. Rev. X 7, 031020 (2017).
- [14] H. J. Liao, Z. Y. Xie, J. Chen, Z. Y. Liu, H. D. Xie, R. Z. Huang, B. Normand, and T. Xiang, Phys. Rev. Lett. 118, 137202 (2017).
- [15] Y.-C. He and Y. Chen, Phys. Rev. Lett. 114, 037201 (2015).
- [16] H. J. Changlani and A. M. Läuchli, Phys. Rev. B 91, 100407 (2015).
- [17] N. Y. Yao, M. P. Zaletel, D. M. Stamper-Kurn, and A. Vishwanath, arXiv:1510.06403.
- [18] D. Yamamoto, G. Marmorini, and I. Danshita, Phys. Rev. Lett. 112, 127203 (2014).
- [19] D. Sellmann, X.-F. Zhang, and S. Eggert, Phys. Rev. B 91, 081104 (2015).
- [20] A. L. Chernyshev and M. E. Zhitomirsky, Phys. Rev. Lett. 113, 237202 (2014).
- [21] O. Götze and J. Richter, Phys. Rev. B 91, 104402 (2015).
- [22] K. Kumar, K. Sun, and E. Fradkin, Phys. Rev. B 90, 174409 (2014).
- [23] K. Kumar, H. J. Changlani, B. K. Clark, and E. Fradkin, Phys. Rev. B 94, 134410 (2016).
- [24] K. Essafi, O. Benton, and L. D. C. Jaubert, Nat. Commun. 7, 10297 (2016).
- [25] T. Momoi and M. Suzuki, J. Phys. Soc. Jpn. 61, 3732 (1992).
- [26] C. D. Batista, Phys. Rev. B 80, 180406 (2009).
- [27] B. S. Shastry and B. Sutherland, Physica (Amsterdam) **108B+C**, 1069 (1981).
- [28] C. K. Majumdar and D. K. Ghosh, J. Math. Phys. (N.Y.) 10, 1388 (1969).
- [29] D. J. Klein, J. Phys. A 15, 661 (1982).
- [30] I. Affleck, T. Kennedy, E. H. Lieb, and H. Tasaki, Phys. Rev. Lett. 59, 799 (1987).
- [31] X.-G. Wen, Phys. Rev. Lett. 90, 016803 (2003).
- [32] A. Kitaev, Ann. Phys. (Amsterdam) 303, 2 (2003).
- [33] H. Wang, H. J. Changlani, Y. Wan, and O. Tchernyshyov, Phys. Rev. B 95, 144425 (2017).
- [34] A. B. Harris, C. Kallin, and A. J. Berlinsky, Phys. Rev. B 45, 2899 (1992).
- [35] C. L. Henley, Phys. Rev. B 80, 180401 (2009).
- [36] D. A. Huse and A. D. Rutenberg, Phys. Rev. B 45, 7536 (1992).
- [37] J. T. Chalker, P. C. W. Holdsworth, and E. F. Shender, Phys. Rev. Lett. 68, 855 (1992).
- [38] S. Sachdev, Phys. Rev. B 45, 12377 (1992).
- [39] O. Cépas and A. Ralko, Phys. Rev. B 84, 020413 (2011).
- [40] C. Castelnovo, C. Chamon, C. Mudry, and P. Pujol, Phys. Rev. B **72**, 104405 (2005).
- [41] See Supplemental Material at http://link.aps.org/supplemental/10.1103/PhysRevLett.120.117202 for several details of the three coloring basis and the analyses of the exact diagonalization calculations.
- [42] R. J. Baxter, J. Math. Phys. (N.Y.) 11, 784 (1970).
- [43] D. L. Bergman, C. Wu, and L. Balents, Phys. Rev. B **78**, 125104 (2008).
- [44] P. W. Leung and V. Elser, Phys. Rev. B 47, 5459 (1993).
- [45] A. M. Läuchli, J. Sudan, and E. S. Sørensen, Phys. Rev. B 83, 212401 (2011).

- [46] F. Kolley, S. Depenbrock, I. P. McCulloch, U. Schollwöck, and V. Alba, Phys. Rev. B 91, 104418 (2015).
- [47] Y. Iqbal, F. Becca, and D. Poilblanc, New J. Phys. 14, 115031 (2012).
- [48] S. Jiang, P. Kim, J. H. Han, and Y. Ran, arXiv:1610.02024.
- [49] A. M. Läuchli and R. Moessner, arXiv:1504.04380.
- [50] I. Rousochatzakis, A. M. Läuchli, and F. Mila, Phys. Rev. B 77, 094420 (2008).
- [51] J. Kondev and C. L. Henley, Nucl. Phys. **B464**, 540 (1996).
- [52] V. Khemani, R. Moessner, S. A. Parameswaran, and S. L. Sondhi, Phys. Rev. B 86, 054411 (2012).
- [53] Y. Wan and M. J. P. Gingras, Phys. Rev. B 94, 174417 (2016).

- [54] J. G. Wright and B. S. Shastry, arXiv:1301.4494.
- [55] Y.-H. Chan and L.-M. Duan, New J. Phys. 14, 113039 (2012).
- [56] B. Normand and Z. Nussinov, Phys. Rev. Lett. 112, 207202 (2014).
- [57] M. Hermele, M. P. A. Fisher, and L. Balents, Phys. Rev. B 69, 064404 (2004).
- [58] D. A. Huse and V. Elser, Phys. Rev. Lett. 60, 2531 (1988).
- [59] H. J. Changlani, J. M. Kinder, C. J. Umrigar, and G. K.-L. Chan, Phys. Rev. B 80, 245116 (2009).
- [60] E. Neuscamman, H. Changglani, J. Kinder, and G. K.-L. Chan, Phys. Rev. B 84, 205132 (2011).

# Supplemental Information for "The mother of all states of the kagome quantum antiferromagnet"

Hitesh J. Changlani,<sup>1,2</sup> Dmitrii Kochkov,<sup>2</sup> Krishna Kumar,<sup>2</sup> Bryan K. Clark,<sup>2</sup> and Eduardo Fradkin<sup>2</sup>

<sup>1</sup>Department of Physics and Astronomy, Johns Hopkins University,

Baltimore, MD 21218 and Institute for Quantum Matter,

Johns Hopkins University, Baltimore, MD 21218

<sup>2</sup>Department of Physics, University of Illinois at Urbana-Champaign,

1110 West Green St, Urbana IL 61801, USA

(Dated: December 10, 2017)

## I. EFFICIENT OVERLAP AND HAMILTONIAN MATRIX ELEMENTS IN THE 3-COLORING BASIS

In the main text, we mentioned the efficient evaluation of the number of linearly independent colorings when projected to definite total  $S_z$  (whose value we denote as  $S_z^*$ ). This number was obtained by diagonalizing the overlap matrix and determining its rank. Here we present expressions for the overlap and Hamiltonian matrices in the  $S_z$  (or number, in the hard-core boson language) projected-coloring basis which correspond to  $S_{CC'} \equiv \langle C|C'\rangle$  and  $H_{CC'} \equiv \langle C|H|C'\rangle$  respectively. A projected coloring  $|C\rangle$  is given by the expression,

$$|C\rangle \equiv P_{S_z} \Big( \prod_i \otimes |c_i\rangle \Big) \tag{1}$$

where  $|c_i\rangle$  is the color on site i and can be  $|a\rangle$ ,  $|b\rangle$  or  $|c\rangle$ , as defined in the main text.

Matrix elements involving projected-colorings are calculated by introducing a complete set of orthonormal states, which for the present purpose is chosen to be the Ising basis, compactly written as,

$$I \equiv \{s_1, s_2, s_3, .... s_N\}$$
 (2)

where  $s_i$  are Ising variables with value  $\pm \frac{1}{2}$  on site i, and N is the total number of sites. Introducing the identity operator we have,

$$\langle C|C'\rangle = \sum_{\text{Iin sector}} \langle C|I\rangle\langle I|C'\rangle$$
 (3)

Naively, this summation may be evaluated only by enumerating all Ising configurations in a given spin sector  $(S_z^*)$  and will thus take an exponentially increasing amount of time to evaluate. However, the Ising sum can be converted to one over unconstrained variables  $s_1, s_2, ... s_N$  and the summation becomes very easy to compute as it factorizes into a product of sums. This is achieved by introducing a delta function and then Fourier transforming the expression as follows,

$$\langle C|C'\rangle = \sum_{I \text{unconstrained}} \langle C|I\rangle\langle I|C'\rangle\delta(S_z - S_z^*) \tag{4a}$$

$$= \frac{1}{N+1} \sum_{p} \sum_{I} \langle C|I\rangle \langle I|C'\rangle e^{ip(S_z - S_z^*)}$$
 (4b)

$$= \frac{1}{N+1} \sum_{p} \prod_{j} \sum_{s_j} e^{ips_j} \langle c_j | s_j \rangle \langle s_j | c_j' \rangle e^{-ipS_z^*}$$
 (4c)

where the sum over p ranges from p=0 to  $p=2\pi N/N+1$  in multiples of  $2\pi/N+1$ . This is because  $S_z$  varies from a minimum of -N/2 to a maximum of N/2. Note that we have used  $S_z = s_1 + s_2 + s_3 \dots + s_N$  to factorize the product into a product of sums.

Associating integers 0,1,2, with the colors a,b,c respectively, it follows that,

$$\langle s_j | c_j \rangle = \frac{1}{\sqrt{2}} \omega^{\left(c_j/2 - c_j s_j\right)}$$
 (5a)

$$\langle c_j | s_j \rangle = \frac{1}{\sqrt{2}} \omega^{\left(c_j - 2c_j s_j\right)} \tag{5b}$$

where  $\omega \equiv e^{\mathrm{i}2\pi/3}$ . In order to simplify the expression of the overlap, we define the variables,

$$\lambda_j \equiv (2c_j + c_j') \pmod{3} = (c_j' - c_j) \pmod{3} \tag{6}$$

and the function,

$$f^{0}(p,\lambda_{j}) \equiv \frac{1}{2} (e^{ip/2} + e^{i2\pi\lambda_{j}/3} e^{-ip/2})$$
(7)

Thus the overlap matrix element reads,

$$\langle C|C'\rangle = \frac{1}{N+1} \sum_{p} F^{0}(p) \tag{8}$$

where we have defined,

$$F^{0}(p) \equiv \prod_{j} f^{0}(p, \lambda_{j}) e^{-ipS_{z}^{*}}$$

$$\tag{9}$$

This equation is correct only up to a normalization factor, because the definition of C and C' does not guarantee an overall normalization automatically. This normalization is just the combined weight on all configurations in the full (unprojected) Hilbert space divided by the combined weight on the configurations in the correct  $S_z$  sector. Including all prefactors into one term we define,

$$\mathcal{N} = \frac{1}{N+1} \times \frac{2^N}{\text{Total Ising configurations in correct sector}}$$
 (10)

which makes the expression for the overlap,

$$\langle C|C'\rangle = \mathcal{N}\sum_{p} F^{0}(p)$$
 (11)

A similar delta function trick can be used in the evaluation of the Hamiltonian matrix elements. For example, the diagonal element in the  $S_z$  basis is  $S_m^z S_n^z$  and can be evaluated as,

$$\langle C|S_m^z S_n^z|C'\rangle = \mathcal{N} \sum_p \left(\frac{f^z(p,\lambda_m)f^z(p,\lambda_n)}{f^0(p,\lambda_m)f^0(p,\lambda_n)}\right) F^0(p) \tag{12}$$

where

$$f^{z}(p,\lambda_{j}) \equiv \frac{1}{4} (e^{ip/2} - e^{i2\pi\lambda_{j}/3} e^{-ip/2})$$
 (13)

The off diagonal element is also straightforward and is found to be,

$$\langle C|S_m^+ S_n^-|C'\rangle = \mathcal{N} \sum_p \left(\frac{f^+(p, c_m') f^-(p, c_n)}{f^0(p, \lambda_m) f^0(p, \lambda_n)}\right) F^0(p)$$
 (14)

where

$$f^{+}(p,c_{j}) \equiv \frac{1}{2}e^{i2\pi c_{j}/3}e^{ip/2}$$
 (15a)

$$f^{-}(p,c_j) \equiv \frac{1}{2}e^{i4\pi c_j/3}e^{-ip/2}$$
 (15b)

These last two expressions do not depend on  $\lambda_j$  but rather the value of the color in the ket or bra.

#### II. COUNTING THE NUMBER OF THREE-COLORINGS

In Table I of the main paper, we showed the number of valid 3-colorings (i.e. colorings which satisfied the constraint of one distinct color per triangular motif) for several lattices. The counting was automated employing a simple divide and conquer algorithm. The lattice was divided into P pieces, and for each piece the number of valid 3-colorings was checked by brute force enumeration of configurations. Then the 3-coloring consistency condition between pieces was checked and the combinations were retained or eliminated accordingly. In practice, for the small lattices considered

here, P=1 to P=6 sufficed, but for larger lattices larger P is possibly needed for efficient counting.

In order to not over-count colorings, it is important to fix the color of one (reference) site to a in all valid colorings. This is because the coloring C', obtained by exchanging the colors (consistently for all sites) of a coloring C, is not linearly independent of it. This can be seen by redefining,

$$|\downarrow\rangle' \equiv \omega|\downarrow\rangle \tag{16}$$

which is equivalent to the transformation (from old to new variables)

$$a \to c$$
 (17a)

$$b \to a$$
 (17b)

$$c \to b$$
 (17c)

Under this transformation each spin configuration (and hence the overall wavefunction) is simply rescaled by a constant factor of  $\omega^{N_{\downarrow}}$  where  $N_{\downarrow}$  is the number of down spins. (A similar transformation holds for  $|\downarrow\rangle' \equiv \omega^2 |\downarrow\rangle$  which leads to  $a \to b$ ,  $b \to c$ ,  $c \to a$ ). Thus, these colorings are not linearly independent and should not be (double or triple) counted.

In Table S1, we show several finite clusters (including those shown in the main text) where the number of 3-colorings were computed and show their correspondence with the number of ground states found from exact diagonalization (ED). The number of linearly independent colorings is the rank (R(S)) of the overlap matrix  $(S_{CC'})$ , whose efficient evaluation was discussed in the previous section.

#### III. 36D CLUSTER

Our results for the kagome phase diagram were based on extensive ED calculations on finite lattices. Since ED is severely limited by size restrictions, it is important to base our conclusions on simulations of a finite cluster which best represents the thermodynamic limit (TDL). The smallest unit cell that can accommodate energetically competitive phases, such as the q=0 and  $\sqrt{3}\times\sqrt{3}$  phases, is known to be the 36d cluster, which has been studied by several authors [1, 2] focused on exploring the Heisenberg point of the XXZ model i.e.  $J_z=1$ . This cluster has D6 as its point group symmetry, which includes reflections and 60 degree rotations. For completeness, in Fig. S1, we show the real space picture of the 36d cluster, along with its reciprocal space.

						_						
Lattice	Method	$n_b = 1$	$n_b = 2$	$n_b = 3$	$n_b = 4$	$n_b = 5$	$n_b = 6$	# 3-colorings				
Finite clusters												
sawtooth obc	ED	6	16	26	31	32	32	32				
length 5	R(S)	6	16	26	31	32	32					
Husimi cactus	ED	5	11	15	16	16	15	16				
generation= 1	R(S)	5	11	15	16	16	15					
21 site kagome	ED	10	44	112	187	231	243	244				
	R(S)	10	44	112	187	231	243					
$3 \times 2$ kagome obc	ED	11	54	156	299	418	474	488				
(23 sites)	R(S)	11	54	156	299	418	474					
$3 \times 3$ kagome obc	ED	15	102	414	1117			3808				
(33 sites)	R(S)	15	102	414	1117	2136	3078					
			Kago	ome on tori	i							
$2 \times 2$	ED	5	8	8	8	8	8	8				
	R(S)	5	8	8	8	8	8					
$3 \times 2$	ED	7	17	17	16	16	16	16				
	R(S)	7	15	16	16	16	16					
$4 \times 2$	ED	9	30	42	33	32	32	32				
	R(S)	9	26	31	32	32	32					
$5 \times 2$	ED	11	47	92	83	65	64	64				
	R(S)	11	42	58	63	64	64					
$3 \times 3$	ED	10	38	60	41	40	40	40				
	R(S)	10	34	40	40	40	40					
$4 \times 3$	ED	13	68	169	172	137	136	136				
	R(S)	13	68	134	136	136	136					
$4 \times 4$	ED	17	122	459	875	793	-	720				
	R(S)	17	122	447	683	719	720					

Table S1. Number of ground states on lattices with triangular motifs calculated from the rank of the overlap matrix of 3-colorings (R(S)) and from exact diagonalization (ED). For all studied clusters and number of hard-core bosons  $(n_b)$  with open boundary conditions (top half), no additional non-3 coloring ground states were found. The kagome clusters had completed triangles, resembling their periodic counterparts. For kagome clusters on tori (bottom half), additional ground states are found at some low fillings.

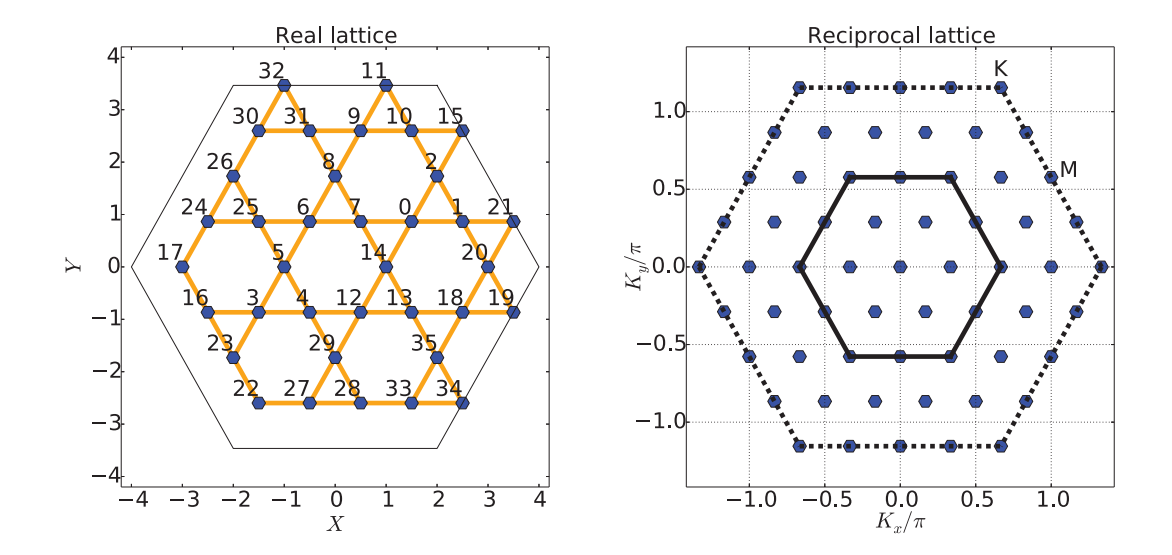


Figure S1. (Color online): 36d simulation cluster (left) and its reciprocal lattice (right) used in the computation of the extended phase diagram. The solid and the dotted lines in reciprocal space show the first and the extended Brillouin zones respectively. The high symmetry points, K and M, of the latter have been indicated.

We work in a fully symmetrized basis which reduces the dimensionality of the Hilbert space for a fully symmetric sector to 63044766 basis elements, which is approximately a factor of 144 smaller than the original  $S_z = 0$  sector. Although the ground state can belong to any irreducible representation and any momentum sector, by analyzing all of the sectors at points  $(J_z, J_2) = \{(-0.3, \pm 0.05), (0, \pm 0.05), (0.1, 0), (0.5, \pm 0.02)\}$  we conclude that it resides in the symmetric sector of K = (0, 0) in the range of interest and focus on investigation of this sector.

We extract several physical quantities from the ground state vectors, such as spin-spin correlation, spin structure factors and ground state fidelity. As an example, the structure factors of the magnetically ordered q=0 and  $\sqrt{3}\times\sqrt{3}$  are presented in Fig. S2.

#### IV. FIDELITY PROFILES FOR $J_2$ SCANS

In Fig. 3 of the main text, we showed the phase diagram for the kagome antiferromagnet in the parameter space of  $J_z$  and  $J_2$ , for the model Hamiltonian,

$$H[J_{z}, J_{2}] = \left(\sum_{\langle i,j \rangle} S_{i}^{x} S_{j}^{x} + S_{i}^{y} S_{j}^{y} + J_{z} S_{i}^{z} S_{j}^{z}\right) + J_{2} \left(\sum_{\langle \langle i,j \rangle \rangle} S_{i}^{x} S_{j}^{x} + S_{i}^{y} S_{j}^{y} + J_{z} S_{i}^{z} S_{j}^{z}\right)$$

$$= H_{XXZ}^{\text{nn}}[J_{z}] + J_{2} H_{XXZ}^{\text{nnn}}[J_{z}]$$
(18)

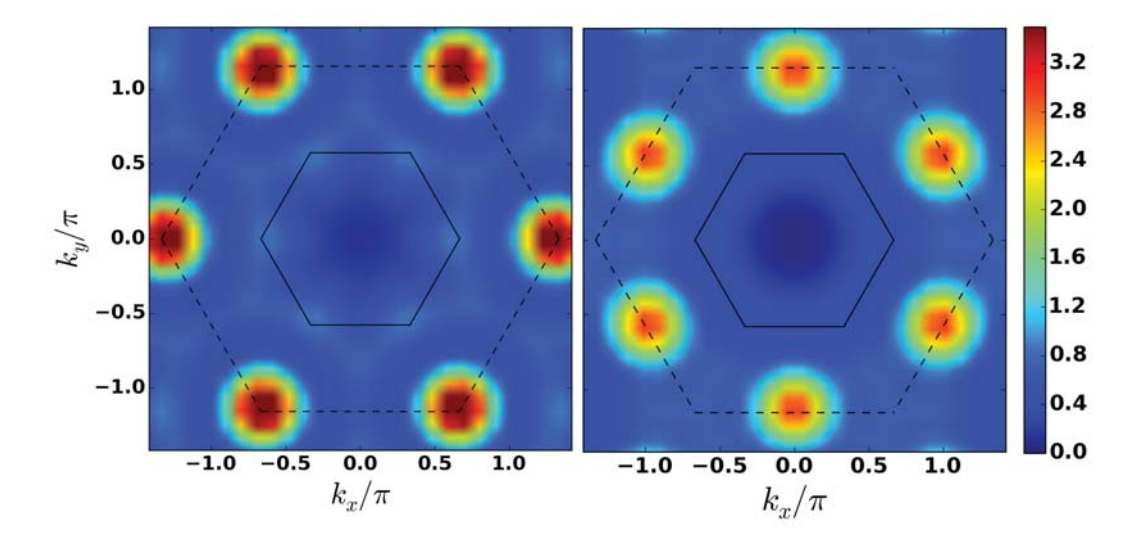


Figure S2. (Color online): Structure factors for magnetically ordered phases  $\sqrt{3} \times \sqrt{3}$  (left) and q=0 (right) computed from Exact Diagonalization at  $J_z=0.1$   $J_2=-0.1$  and  $J_z=0.1$   $J_2=0.1$  respectively. For  $J_2<0$ , the intensity is maximum at the K points of the extended Brillouin zone and for  $J_2>0$  it is maximum at the M points.

where  $\langle i, j \rangle$  and  $\langle \langle i, j \rangle \rangle$  denote the nearest neighbor (nn) and next-nearest-neighbor (nnn) sites respectively.

Our estimates of the phase boundaries were based on the measuring fidelity of the ground state wavefunction  $\psi(J_z, J_2)$ , by scanning in the  $J_2$  direction (keeping  $J_z$  fixed),

$$f(J_z, J_2) \equiv \left| \langle \psi(J_z, J_2 - \Delta J_2/2) | \psi(J_z, J_2 + \Delta J_2/2) \rangle \right|$$
(19)

where  $\Delta J_2$  is the step size. Dips in the fidelity profile indicate the existence of phase transitions.

Our results for representative  $J_z$ , with  $\Delta J_2 = 0.01$  are shown in Fig. S3. We observe that there are prominent dips for  $J_2 < 0$  and  $J_2 \approx 0$  and only a marginal one for  $J_2 > 0$ . The location of of both the leftmost and rightmost dips increases in  $|J_2|$  on increasing  $J_z$ , this corresponds to the appearance of the wedge in the kagome phase diagram in Fig. 3. Prominently, the dip at  $J_2 \approx 0$  is present for all  $J_z$  shown.

#### V. FERROMAGNET AND BOUNDARIES SHARED WITH ADJOINING PHASES

In this section of the supplement, we discuss certain aspects of the ferromagnetic (FM) region reported in Fig. 3 of the phase diagram and the phase boundaries it shares with its adjoining phases.

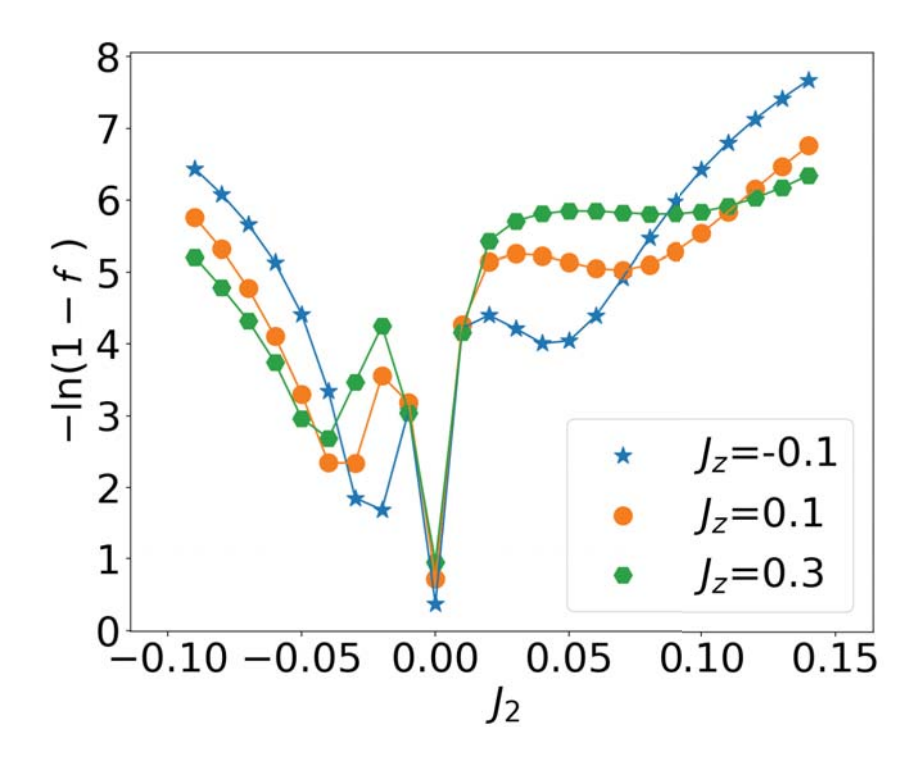


Figure S3. (Color online) Fidelity scans along the  $J_2$  axis for different values of  $J_z$ . The fidelity is evaluated for ground state wavefunctions at parameter values which differ by  $\Delta J_2 = 0.01$  (keeping  $J_z$  fixed). The spreading location of the leftmost and rightmost dips (increase in  $|J_2|$ ), as  $J_z$  is increased, corresponds to the wedge feature in the kagome phase diagram.

Moving along the direction of  $J_z < -0.5$  lifts the exponential degeneracy to favor the fully polarized sector. Therefore, in the  $S_z = 0$  sector, the energy density (energy per site) is minimized by the phase separated FM state which has half the system (N sites) maximally polarized up ( $S_z = N/2$ ) and the other half maximally polarized down ( $S_z = -N/2$ ). This can be proven analytically, since the fully polarized state simultaneously generates the minimal possible energy for all four terms of the Hamiltonian (XXZ0 of the triangles made of nearest neighbor bonds,  $J_2XXZ0$  of the triangles made of next nearest neighbor bonds,  $(J_z+1/2)\sum_{\langle i,j\rangle} S_i^z S_j^z$  and  $J_2(J_z+1/2)\sum_{\langle i,j\rangle} S_i^z S_j^z$  for  $J_2 \geq 0$ . Phase separation results in a domain wall which costs absolute energy but, in the TDL, costs zero energy per site for short-ranged Hamiltonians such as ours. While it is possible there are other states with the same energy density but lower absolute energy for a finite system, we see no evidence of this. While a large enough simulation will exhibit emergent phase separation, finite size effects dominate in a small ED calculation. Nonetheless, in

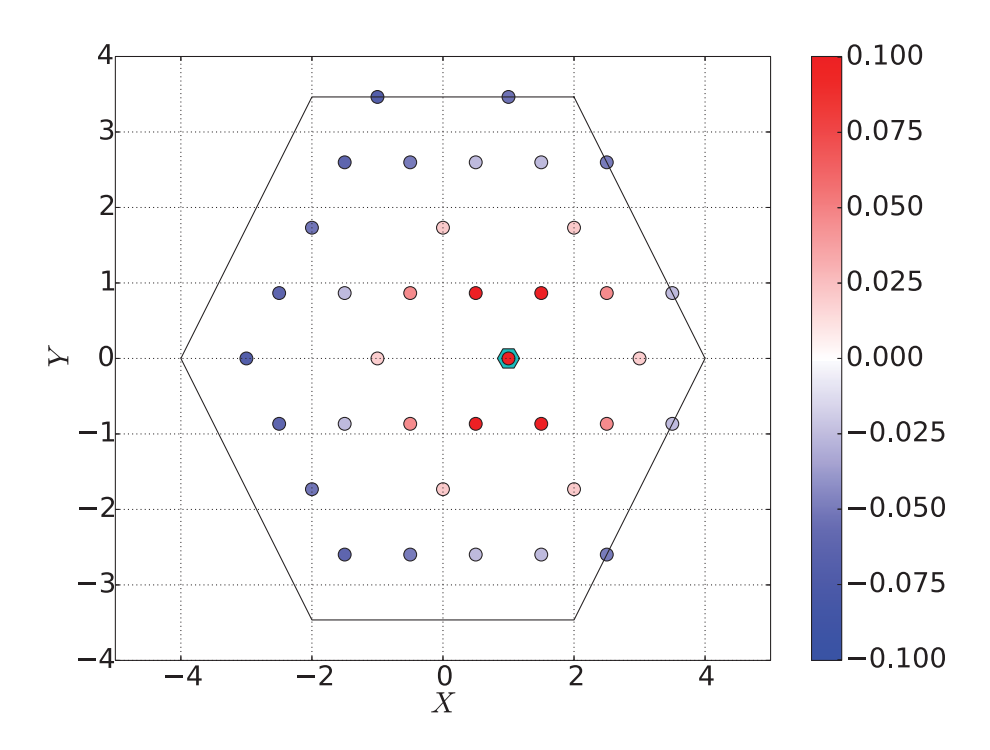


Figure S4. (Color online): ZZ component of the real space spin-spin correlation function (with respect to a reference site) in the  $S_z = 0$  ground state at  $J_z = -0.7$ ,  $J_2 = 0$ . The cyan hexagon marks the lattice site with respect to which the correlation function is computed. The color represents the correlation strength (red - ferromagnetic, blue antiferromagnetic correlations).

most (but not all) of the region  $J_z < -0.5, J_2 > 0$  we see clear phase separation in the spin-spin correlation function such as at  $J_z = -0.7, J_2 = 0.0$ , see Fig. S4.

Let us now consider the lines separating the q=0 and FM (the vertical line  $J_z=-1/2$  for  $J_2\geq 0$ ) and the  $\sqrt{3}\times\sqrt{3}$  and FM regions, the latter calculated to be,

$$|J_z| = \frac{\left(\frac{1}{2} + |J_2|\right)}{\left(1 - |J_2|\right)} \tag{20}$$

Both boundaries can be understood by comparing the semiclassical energy of the unprojected magnetically ordered states with that of the FM. For example, the energy associated with four nearest neighbor and four next nearest neighbor bonds emanating from a single site in the FM state is  $-4|J_z|+4|J_2||J_z|$  in comparison to  $4(-1/2)-4|J_2|$  for the unprojected coplanar  $\sqrt{3}\times\sqrt{3}$  state. The phase boundary of these two phases is shown by the solid line in Fig. 3 of the main text and corresponds to Eq. (20). Similarly, the q=0 energy is higher than the FM for  $J_z<-1/2$  for any  $J_2>0$ . We note that despite involving only semiclassical arguments, the agreement of

these phase boundary estimates with those obtained from energy densities calculated from ED, is excellent.

#### VI. HAMILTONIAN WITH FOUR COLORING EXACT GROUND STATES

We noted that the idea of coloring wavefunctions generally applies to beyond triangular motifs. Here we explicitly write down the Hamiltonian for which the four coloring wavefunction is an exact ground state on lattices with motifs involving four sites (such as the square, checkerboard and pyrochlore lattices). We derive this Hamiltonian for the case of four sites; the extension to the case of lattices with *shared* four colorable motifs is trivial.

First, define the four colors as,

$$|a\rangle \equiv |\uparrow\rangle + |\downarrow\rangle \tag{21a}$$

$$|b\rangle \equiv |\uparrow\rangle + i|\downarrow\rangle \tag{21b}$$

$$|c\rangle \equiv |\uparrow\rangle - |\downarrow\rangle \tag{21c}$$

$$|d\rangle \equiv |\uparrow\rangle - i|\downarrow\rangle \tag{21d}$$

Then define the states,

$$|1\rangle \equiv |\downarrow\uparrow\uparrow\uparrow\rangle + |\uparrow\downarrow\uparrow\uparrow\rangle + |\uparrow\uparrow\downarrow\uparrow\rangle + |\uparrow\uparrow\uparrow\downarrow\rangle \tag{22a}$$

$$|2\rangle \equiv |\uparrow\uparrow\downarrow\downarrow\rangle + |\uparrow\downarrow\uparrow\downarrow\rangle + |\uparrow\downarrow\downarrow\uparrow\rangle + |\downarrow\uparrow\uparrow\downarrow\rangle + |\downarrow\uparrow\uparrow\uparrow\rangle + |\downarrow\downarrow\uparrow\uparrow\rangle$$
 (22b)

$$|3\rangle \equiv |\uparrow\downarrow\downarrow\downarrow\rangle + |\downarrow\uparrow\downarrow\downarrow\rangle + |\downarrow\downarrow\uparrow\downarrow\rangle + |\downarrow\downarrow\downarrow\uparrow\rangle \tag{22c}$$

Then, any Hamiltonian of the form

$$H = \lambda_1 |1\rangle\langle 1| + \lambda_2 |2\rangle\langle 2| + \lambda_3 |3\rangle\langle 3| \tag{23}$$

with  $\lambda_1, \lambda_2, \lambda_3 \geq 0$  will have the coloring wavefunction  $|C\rangle = |a\rangle \otimes |b\rangle$ .... as an exact ground state with zero energy as long as one satisfies the constraint of one a, b, c, d each per four-site motif. Here we present the result for  $\lambda_1 = \lambda_2 = \lambda_3 = 1$ , where H is also time reversal invariant.

We used the DiracQ package [3] to simplify the spin algebra and up to an overall scale factor found the Hamiltonian to be,

$$H = \frac{7}{8} + \left(\sum_{i < j} S_i^+ S_j^- + S_i^- S_j^+ - \frac{1}{2} S_i^z S_j^z\right) + \sum_{i < j, k < l, \text{diff}} S_i^+ S_j^+ S_k^- S_l^- - 2 S_1^z S_2^z S_3^z S_4^z \quad (24)$$

where the notation "diff" is used to indicate that all the indices i, j, k, l are distinct.

\_\_\_\_

- [1] P. W. Leung and V. Elser, Phys. Rev. B 47, 5459 (1993).
- [2] A. M. Läuchli, J. Sudan, and E. S. Sørensen, Phys. Rev. B 83, 212401 (2011).
- [3] J. G. Wright and B. S. Shastry, ArXiv e-prints (2013), arXiv:1301.4494 [cond-mat.str-el].